Available online at www.rilem.net

Materials and Structures **38** (March 2005) 257-266

Mechanical response of solid clay brickwork under eccentric loading. Part I: Unreinforced masonry

A. Brencich and L. Gambarotta
Department of Structural and Geotechnical Engineering, University of Genoa, Italy

Received: 10 October 2003; accepted: 19 April 2004

ABSTRACT

The compressive strength of eccentrically loaded masonry, affecting the strength of arches, vaults, pillars and out-of-plane loaded masonry panels, is addressed in this paper both from the experimental and numerical point of view. The aim is that of relating the eccentric compressive strength to the concentric value, to the mechanical characteristics of the constituents, *i.e.* mortar and bricks, and to the brickwork bond. In the paper, displacement controlled compression tests on solid clay brick and cement-lime mortar masonry prisms, under concentric and moderate-to-highly eccentric loading, are presented and discussed. The experimental outcomes and the results of FEM models give a preliminary insight in the mechanical response of masonry up to collapse. It is found that edge effects may affect the load carrying capacity of the brickwork, while detailed measurements on the mortar joints show that the plane section assumption, typical of many design procedures, is reasonably verified up to the limit load, giving way to simplified but reliable design procedures.

RÉSUMÉ

La résistance à compression dans les murs chargé excentriquement, typique des arches, des voûtes, des piliers et des panneaux de murs charges hors de leurs propres étages est prise en considération dans ce travail d'un point de vue expérimental et numérique. Le but est de trouver une relation entre la résistance à compression excentrique et celle centrée et les caractéristiques mécaniques des composants, par exemple mortier et briques avec la texture de la maçonnerie. Dans l'étude, on présente et on discute les preuves de compression en contrôlant la compression sur les prismes des briques pleines et mortier de chaux et ciment. Les résultats expérimentaux et ceux des modèles FEM fournissent quelques informations sur les réponses mécaniques des murs jusqu'à leur effondrement. On s'est rendu compte que les effets de bord peuvent influencer la capacité de résistance de la maçonnerie alors que des mesures détaillées sur les joints de mortier démontrent que les hypothèses de conservation des sections plates, selon différentes façons de calculer, sont vérifiées raisonnablement jusqu'à la limite de la charge, ouvrant la route à des façons de calculer plus simples mais fiables.

1. INTRODUCTION

The typical stress distribution in masonry structural elements is due to eccentric loading conditions; this can be found in pillars, out-of-plane loaded walls, vaults and arches of historical and ordinary buildings and of masonry bridges.

In several cases, the collapse of eccentrically compressed masonry structures shows the activation of localised flexural mechanisms, the so called *plastic hinges*, *i.e.* sections in which the compressed part of the arch crushes and the mortar joints at the opposite side open, Fig. 1. A detailed analysis of the plastic hinge recognizes a compressed part, near the open part of the mortar joint, which is not yet crushed and in which a non linear response of the material and inelastic strains are likely to be assumed. But, in spite of these evidences, the mechanical model for masonry is still a debating issue and substantially different mechanical models are still used in the assessment procedures for arch-type structures. In some approach [1-5] masonry is assumed a No Tensile Resistant (NTR) material rigid in compression; in this way the collapse of the structure is implicitly assumed to be almost independent on the compressive strength of the brickwork. In other more detailed models, both limit analysis [6, 7] and incremental iterative procedures [8], masonry is represented as an elastic-perfectly plastic material with limited inelastic strains and the compressive strength is assumed either coincident with the value for concentric loading or a model parameter to be identified through some experimental test. Other models [9-11], mainly looking at simplified limit state approaches, are somewhere in-between since they assume a NTR constitutive model and set the compressive strength as a parameter depending on the load eccentricity.

doi:10.1617/14134

Fig. 1 - Plastic hinge developed in the arch barrel of a collapsed bridge on the Scrivia river (Alessandria, Italy).

Whatever the approach, the issue is that of the mechanical response of masonry and of relating its compressive strength under eccentric loading to the value under concentric loading. In the frame of an assessment procedure for eccentrically loaded masonry, *i.e.* out-of-plane loaded walls and vaults, reference is made to the constituents since mechanical data are much more easily obtainable for bricks and mortar of an existing bridge rather than for its brickwork.

A reference approach has been developed for concentrically loaded masonry. Due to the doubly periodical distribution of bricks and joints and, consequently, of the stress state, the compressive strength may be expressed in terms of the mean stress provided a local collapse condition is given and proper homogenization techniques are used to derive an equivalent homogeneous material [12-16]. A simplified approach to masonry [17, 18] assumes a simply periodic model, *i.e.* a layered unlimited continuum for which the compressive strength can be deduced from the mechanical properties of the units and of the mortar on the basis of local stress limit conditions and on limit analysis approaches [19-24], the results being in reasonable agreement with the experimental data [22, 24].

Under eccentric loading the periodicity of the stress state is lost, at least through the thickness of the structural element, so that this approach is not applicable and the compressive strength and the collapse mechanisms remain open issues.

Moreover, the only available approach to this problem is provided by the FICHE-UIC recommendations [35] and few experimental outcomes [10, 11, 24], mainly focused on the load carrying capacity of the structural brickwork rather than on the effective collapse mechanism. The only detailed tests specifically related to eccentric loading [25] refer to dry assemblages of stone blocks, which makes these data not very useful for solid clay brickwork.

In order to get a better understanding of the effect of the load eccentricity on the masonry strength and its collapse mechanisms, preliminary to the formulation of proper mechanical models related to the single constituents and their characteristics, a series of experimental tests have been performed on short prisms (5.5x11x24 cm solid clay bricks and 1:1:5 cement-lime mortar) representing a generic section of an arch-type structure. The prisms are 24 cm large, 11 cm thick and 27 cm high, with height-to-width ratio approximately equal to 1 in order to reduce the effects of lateral deflection [24]. The load eccentricity ranges from 0 to 5/12 of the section height so that moderately-to-highly non uniform compressive stresses have been investigated. FEM analyses allow some interpretation of the collapse mechanisms of the brickwork and, along with the experimental data, can be considered as a first glance in the mechanical response of eccentrically loaded masonry. Besides, comparisons with other mechanical models give way to some considerations on the limits of the classical continuum approaches to masonry arch-type structures.

2. TESTING PROCEDURE

The masonry prisms consist of four 5.5x11x24 cm bricks and five 10 mm thick mortar joints of 60 days of age; the upper and lower mortar joints are in direct contact with two steel plates, Fig. 2, the lower one being fixed to the testing setup. The plates are loaded through cylindrical hinges allowing the load line to be precisely set.

Displacements are measured by means of mechanical devices with a 1/100 mm precision (1/1000 mm precision for testing the materials) in three different points directly on the plates (bases 1, 2 and 3) in order to quantify the total displacement of the steel plates and their relative rotation. The central joint is controlled in six positions, two at the extremities (4 and 5) and two on each side of the specimen at $1/4^{th}$ and $3/4^{th}$ of the brick length (6 and 7 on one side, 8 and 9 on the opposite one). The devices are connected to the specimen by means of screw bolts glued with epoxy resin in the brick, Fig. 3.

The moving end of the machine (upper part) is displacement controlled, while the load is measured through the load cell, a C5 class *HBM-RTN* load cell with a 0.01% precision located in-between the upper plate and the machine. In this way, the load process is substantially a displacement-

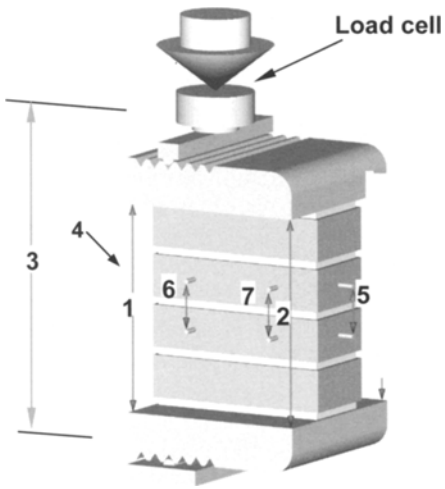

Fig. 2 - Testing setup.

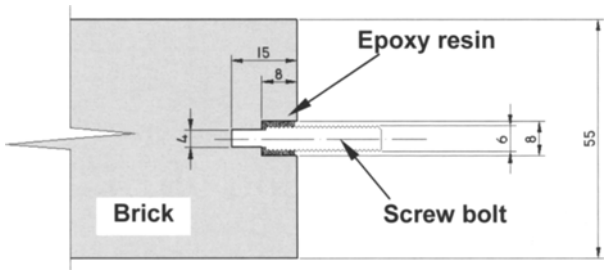

Fig. 3 - Connection of the measuring device to the brick.

controlled procedure; the plates are free to rotate only around the hinges while the other rotation, normal to the hinge axis, is locked by the experimental setup. The load cell can be considered as a spring with high stiffness.

Some of the material properties have been measured in direct compression tests, according to EN196 standards, under displacement controlled loading and by means of a testing setup similar to that of Fig. 2 but for the load cell (50 kN C5 class AEP-TCE cell with a 0.01% precision) and the overall dimensions. Mortar specimen have been adequately vibrated, manufactured and cured in steel boxes. Tables 1 and 2 summarize the main mechanical parameters measured for the materials.

The tensile strength has been defined as the average over three TPB tests. The 1:1:5 cement-lime mortar was intended to represent a medium strength European mortar, whilst the outcomes show a rather high compressive strength. The tensile strength for mortar turned out to be higher than the expected value of 1/10 of the compressive strength; this is probably because the indirect flexural tensile strength measured by a 3 PBT is higher than the direct tensile one, to which a mechanical model usually refers.

The elastic modulus and the Poisson's ratio of the mortar specimen, on the other side, cannot be measured on the small specimen suitable to test the compressive strength (4x4x4cm). For this reason, the Poisson's ratio of mortar had to be deduced from literature [26], while the elastic modulus of mortar was given a value so as to reproduce the global elastic modulus of masonry. In the elastic part of the response, under concentric loads, the equivalent modulus for masonry E_M can be evaluated in terms of the mechanical parameters of the different materials on the basis of the phase rule [18]:

$$\frac{1}{E_M} = \frac{\eta_b}{E_b} + \frac{\eta_m}{E_m} + 2\eta_m\eta_b \frac{\nu_b E_m - \nu_m E_b}{\eta_m(1-\nu_b)\ E_m + \eta_b(1-\nu_m)E_b}\left(\frac{\nu_m}{E_m^2} - \frac{\nu_b}{E_b^2}\right) \quad (1)$$

where $\eta_m = t_m/(t_m + t_b)$, $\eta_b = t_b/(t_m + t_b)$ are the volume fractions of mortar and brick and t_m and t_b are the respective thickness, while E_b, ν_b, E_m and ν_m, are the elastic modulus and Poisson's ratio of brick and mortar respectively. Equation (1) originates from the layered continuum model; the third term, coupling mortar and brick properties, contributes for less than 1% to the global elastic modulus. In this way Equation (1) turns out to be quite insensitive to the values of the Poisson's ratio. The tensile strength was defined according to established data [27].

Once the mechanical parameters for brick and Poisson's ratio of the mortar are given, the elastic modulus for mortar

Table 1 - 1:1:5 Mortar mix for the two series of specimens

Series n.	Sand		Water		Cement	Water/ /Cement	Lime
	Dry weight	Water content	Added	Total			
1	67 N	1.8 *l*	6.8 *l*	8.6 *l*	13 N	6.4	13 N
2	65 N	2.0 *l*	3.8 *l*	5.8 *l*	13 N	4.4	13 N

Table 2 - Experimental data for the materials

Solid clay BRICKS							
Specimen n.	1	2	3	4	5	6	**av.**
Compressive strength f_c [MPa] (direct)	19.97	16.31	19.32	19.68	24.27	/	**19.90**
Tensile strength f_t [MPa] (indirect – TPB tests)	3.11	3.40	3.38	3.65	3.42	/	**3.39**

1:1:5 cement-lime MORTAR	series n. 2					series n. 1		
Specimen n.	1	2	3	4	**av.**	5	6	**av.**
Compressive strength f_c [MPa] (direct)	14.04	15.38	14.55	14.91	**14.72**	11.28	11.50	**11.39**
Tensile strength f_t [MPa] (indirect – TPB tests)	4.38	4.47	4.81	3.11	**4.19**	3.52	3.08	**3.30**

Table 3 - Mechanical parameters for brick and mortar (experimental data and assumptions)

BRICK			MORTAR		
Property	**Value**	**Notes**	**Property**	**Value**	**Notes**
E_b [N/mm^2]	2400±200	Direct compression - average on 3 specimens	E_m [N/mm^2]	335	see text
ν_b	0.05±0.007	Direct compression - average on 3 specimens	ν_m	0.2	Rots [26]
f_t [N/mm^2]	3.4±0.25	TPB - average on 3 specimens	f_t [N/mm^2]	1.4	Brencich *et al.* [27] – see text
f_c [N/mm^2]	18.7±2.1	Direct compression - average on 6 specimens	f_c [N/mm^2]	14.7±0.6	Direct compression - average on 6 specimens

has been assumed so as to reproduce the global modulus for masonry as deduced from the experimental tests. The overall mechanical parameters are given in Table 3. The elastic modulus of the brick fits well other experimental data on similar materials [28] showing that clay brick units can exhibit unexpectedly low elastic moduli.

Finally, it has to be noted that no frictionless device has been adopted, such as steel brushes [30] or PTFE sheets, even though friction between the steel plates and the specimen is known to affect the compressive strength and the collapse mechanism of the specimen. This choice is due to the problems that could arise under eccentric loading, when the specimen could undergo uncontrolled sliding phenomena.

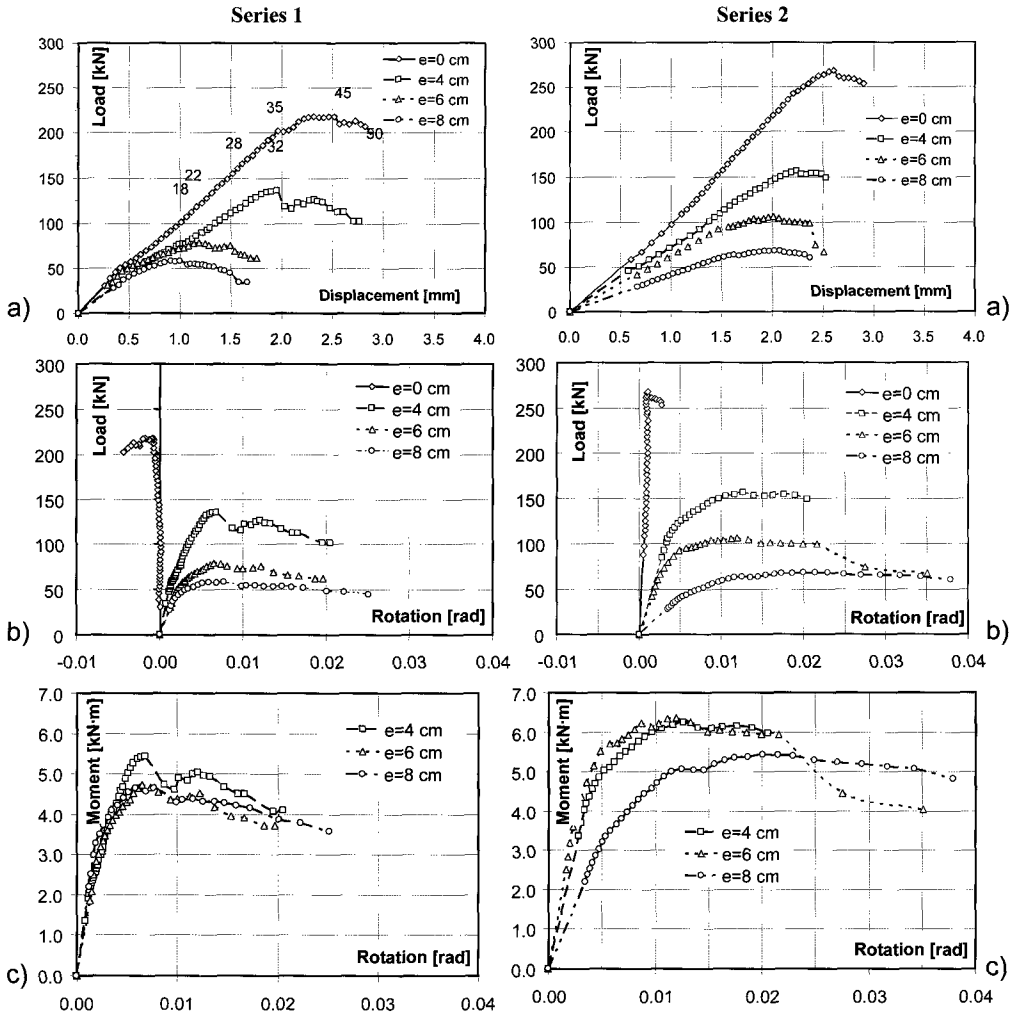

Fig. 4 - a) Load-Displacement, b) Load-Rotation and c) Moment-Rotation curves. Left column: series 1; right column: series 2. Eccentricity is measured in cm.

3. TEST RESULTS

Two series of specimens have been tested, differing in the water content of mortar, Table 1, so that every test could have been replicated twice. Five different eccentricities have been tested: e/h = 0, 0.18, 0.27, 0.36, 0.45, h being the section height; the highest value gave uncertain results and only the ultimate load and displacement were recorded. In each of the other tests, load-displacement, load-rotation and moment-rotation curves have been recorded, Fig. 4; for e/h=0 (concentric loading) no significant rotation was found, as it should, up to the limit load point.

The softening phase was quite long; the last point of the diagrams of Fig. 4 simply marks the end of the meaningful part of the test and does not stand for the sudden collapse of the specimen. Both the tests with the whole section compressed (e/h = 0 and e/h = 0.18) show a significantly linear initial response; on the other hand, under highly eccentric loading conditions the non-linear response is evident. Table 4 summarizes the main results from the tests.

The elastic modulus of the masonry assemblage under concentric loading (estimated equal to 12300 N/mm^2) fits reasonably well with other laboratory [28] and *in-situ* tests on Italian historical railway bridges [31].

The displacements across the central mortar joint, bases 4 to 9, have been recorded throughout the test and are represented in Fig. 5 for the eccentric loading. The different lines represent the position of the joint at various load levels. The percentage is referred to the strain attained at the maximum load, so that figures over 100% indicate the softening phase and below that values indicate the pre-peak response. The experimental profiles of the central joint show that the cross section remains substantially plane up to the peak load; once the limit point is reached, the compressed part of the section crashes, but the remaining part is still plane, at least on the average.

Table 4 - Concentrically loaded prisms – main data of the tests

Concentric loading	Compr. strength f_c [MPa]	El. modulus E [MPa]	El. strain ε_{el}	Ult. strain ε_{ul}	Ductility $\delta_{ul}=\varepsilon_{ul}/\varepsilon_{el}$
Series n. 1	9.9	1260	0.0074	0.0105	1.42
Series n. 2	13.5	1620	0.0088	0.0107	1.20

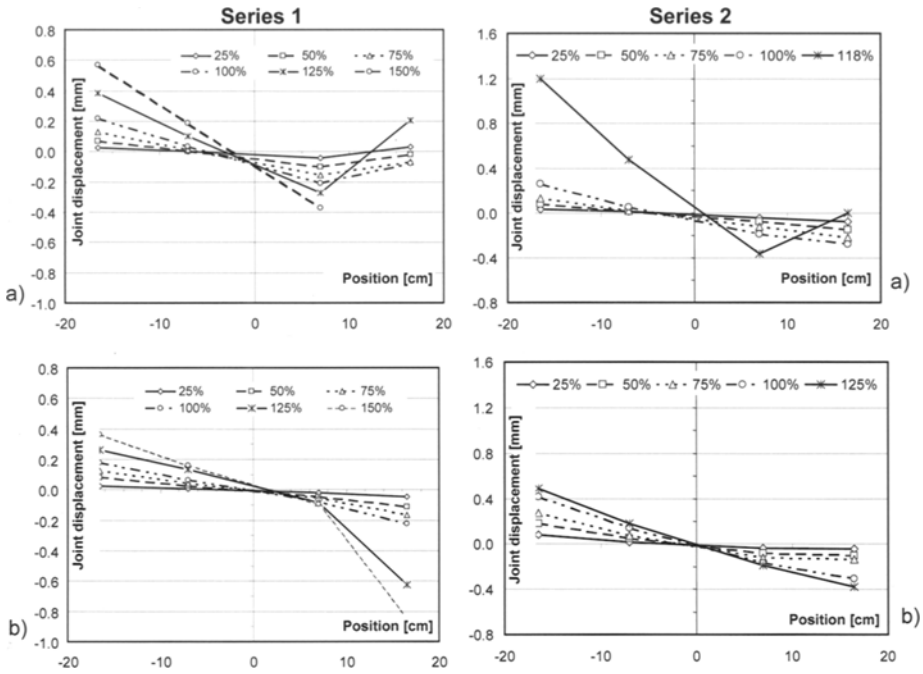

Fig. 5 - Position of the central joint for a) e/h=0.27 and b) e/h=0.36. Left column: series 1; Right column: series 2.

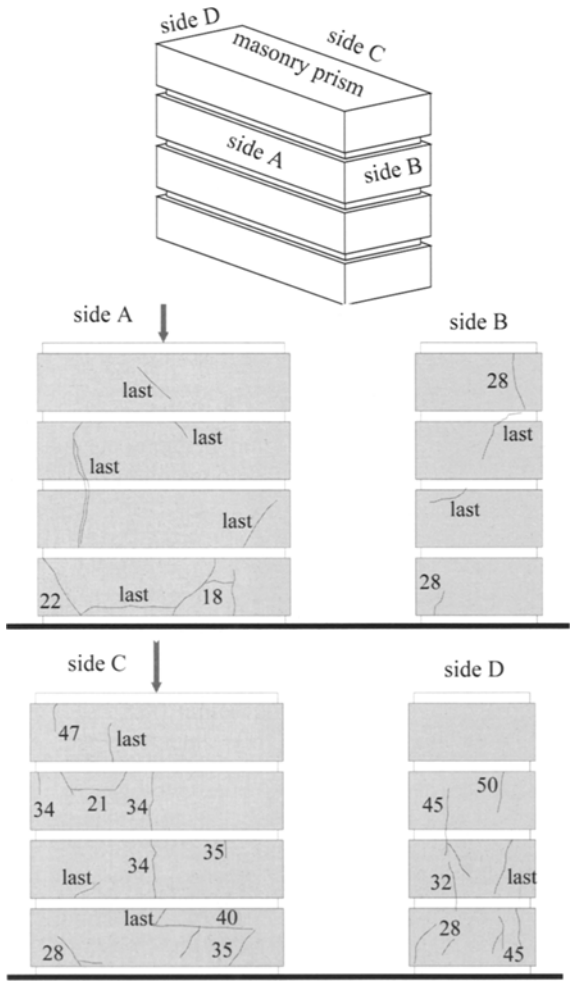

Fig. 6 - Crack pattern for concentric loading – the numbers indicate the load step at which the crack was detected.

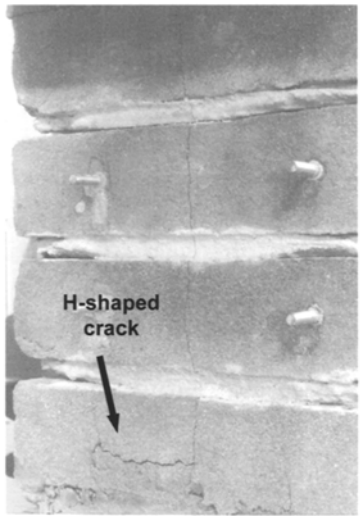

Fig. 7 - Concentric loading – side C bottom: spalling of the outside part of the brick. White arrows indicate the typical H-shape pattern.

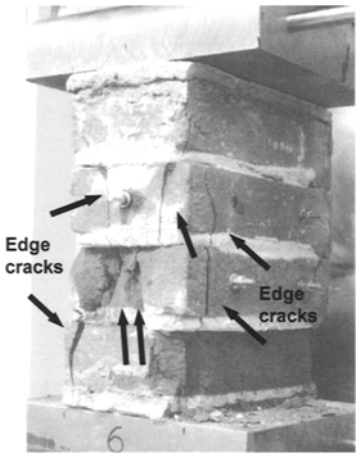

Fig. 8 - Concentric loading – side D/C: internal cracking after removal of the detached parts. The double arrows indicate an internal core less damaged than the external part. Some evidences of external peeling.

Fig. 6 represents a typical crack pattern (numbers refer to the load step at which the crack appeared), while Figs. 7 and 8 show the specimen at the end of the test before and after removal of the cracked parts of the bricks. The H-shaped crack pattern of Fig. 7 is due to the lateral instability of a thin sheet of brick; in Fig. 8 this thin sheet has been removed (right bottom hand side) showing that a crack almost parallel to the surface had developed; many other cracks indicate that such a phenomenon takes place also in the central bricks. The inner core seems to be less damaged than the external parts of the brick; cracks extend to the mortar joint only when some parts of the brick are detached.

It has to be noted that the measuring devices and their connections to the prisms never activated cracking. In fact, also up to the final stage of collapse, neither a screw bolt originated any crack.

4. FEM MODELLING OF MASONRY

A FEM analysis (ANSYS 5.7) of the mortar-brick stack could help in understanding the inner mechanisms and the cracking phenomena inside the bricks and the mortar joints.

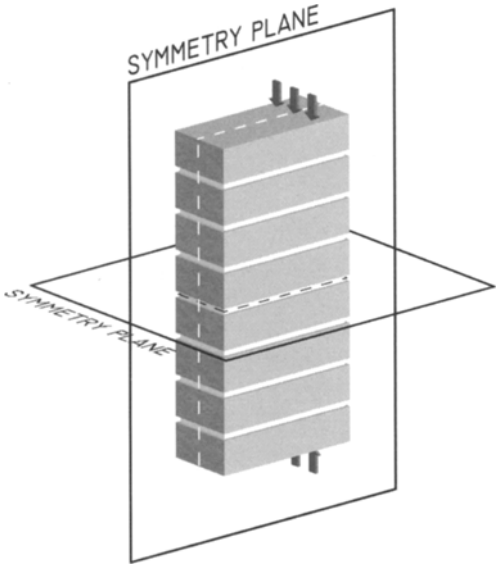

Fig. 9 - Symmetry conditions of an infinite stack of mortar joints and brick units.

The symmetry conditions of an assemblage of mortar joints and bricks, Fig. 9, allow the analysis of the specimen to be limited to $1/4^{th}$ of the joint/brick fundamental unit only. The material model, for both fired clay and mortar, is assumed isotropic with the mechanical characteristics specified in Table 2. The assumed failure rule for both the materials is the Willam-Warnke three-parameters model [32] which had been developed for concrete but, nevertheless, it has been successfully used for brittle materials, such as mortar, fired clay and also masonry as a whole [33]. In order to represent the strong stress gradients, the mesh is quite dense approximately 34.000 dofs. for $1/8^{th}$ of the brick/mortar assemblage with an average F.E. dimension equal to 3 mm. Since there is experimental evidence that no sliding takes place at the mortar/brick interface, probably due to the high compressive vertical stresses, the brick/mortar interface is modelled as a pure contact surface that may open under tensile stresses.

4.1 Concentric loading

Fig. 10 compares the load/displacement response of FEM models, differing for the tensile strength of the brick, to the measured experimental data; the agreement remains good up to 90% of the collapse load. The good agreement in the elastic phase should not be considered of great significance since the elastic modulus of the mortar has been chosen, via Equation (1), exactly to fit the global average elastic modulus of the prism. The collapse load of the FEM model with a 3.4 N/mm^2 tensile strength, the value measured in the TPB test, is very close to the experimental value.

Fig. 11 a shows the very beginning of the cracking phenomenon (arrows in Fig. 10 indicate the points at which cracking activated in the FEM models) at approximately 90% of the ultimate load, while Fig. 11 b plots the distribution of cracks at a 96% load level. The first cracks appear inside the brick close to the brick/mortar interface as a consequence of the elastic mismatch between brick and mortar and do not extend into the mortar joint, in agreement with the classical

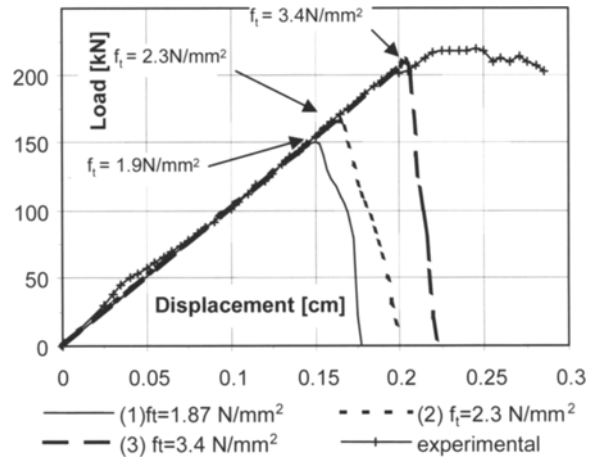

Fig. 10 - Load/displacement curves for the theoretical model with different eccentricities of the load (displacement for a 270 mm long stack).

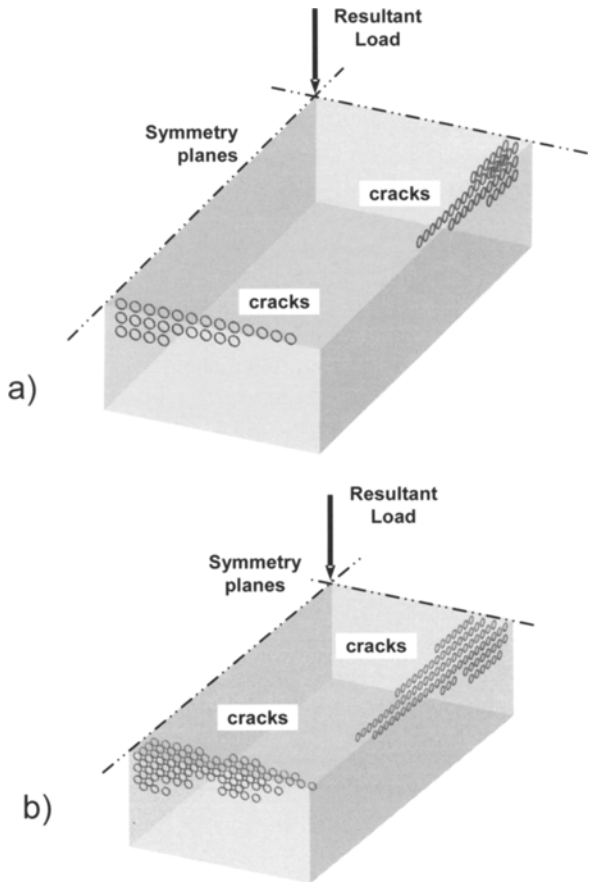

Fig. 11 - Crack distribution in upper part of the brick in the neighbourhoods of the free edges: a) at the very beginning of crack propagation; b) at approximately 90% of the ultimate load.

elastic [18-20] and limit [21, 22] theories. Cracks are formed parallel to the brick sides and in the neighbourhood (5-10 mm) of the external free edges; they develop inside the brick towards its centre, tending to separate an exterior thin sheet from the inner core of the brick. The activation of cracks is well explained by the stress distribution inside the brick; whilst

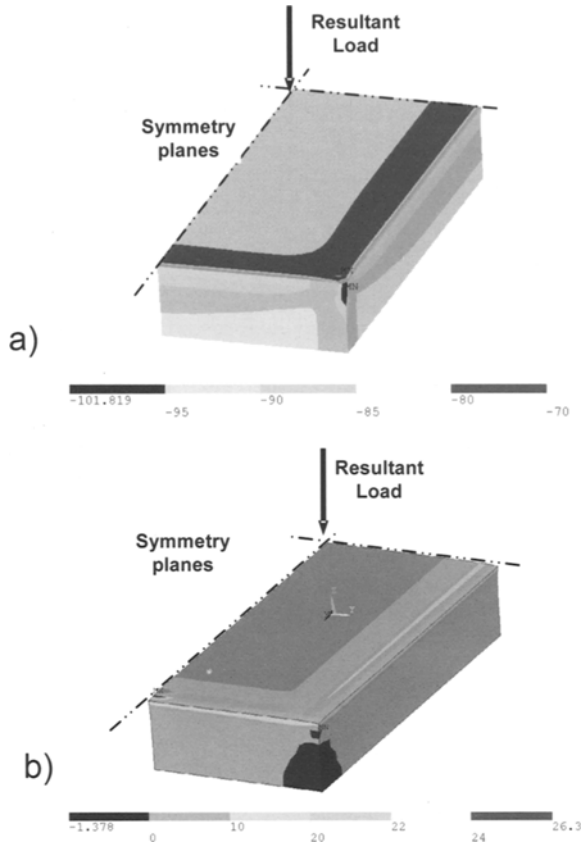

Fig. 12 - Distribution of the a) vertical and b) principal tensile stresses at the initiation of the first cracks [N/mm^2*10]. Upper part of the brick.

vertical stresses, Fig. 12 a, are rather uniform (8-8.5 N/mm^2) with a partial relief (7-7.5 N/mm^2) close to the edges, the principal tensile stresses in the brick are concentrated in a narrow strip 5-10 mm from the exterior face of the brick, Fig. 12 b, just in the area where cracks are first formed.

The major difference arises in the post-peak phase: the experimental evidence shows a limited but clear softening phase while FEM models foresee a catastrophic collapse, Fig. 10, probably due to the cohesive model adopted for the tensile stress transfer across the crack surfaces: while FEM codes assume a sudden drop in the stress transfer across the crack faces, it is much more likely to expect a gradual decrease in reality. As it has been observed, cracking activates close to the external surfaces and concentrates in a rather limited volume; when cracks spread across the brick, the exterior part tends to detach from the inner core and the FEM models loose convergence. Collapse, therefore, is attained when cracking passes through the brick thickness, with a sudden drop in the load carrying capacity of the brick/mortar assemblage, and turns out to be a local phenomenon close to the free surfaces, as already conjectured by Rots [26]. It is worthwhile noting that cracking does not affect the mortar joint, in agreement with experimental tests showing that the joints are not directly involved in the activation of masonry collapse.

If we assume the central part of the brick, where FEM analyses foresee an almost uniform stress distribution, as its load carrying part, the inner core of the brick, Fig. 8, is identified also in the numerical model. This fact, due to the stress concentration close to the external surface of the brick, is in contrast with one of the basic assumptions of the elastic [10-12] and limit-analysis based models [13, 14], *i.e.* with the hypothesis of a uniform distribution of tensile stresses throughout the brick thickness.

4.2 Eccentric loading

The FEM results for eccentric loading is here discussed for an eccentricity of 6 cm only, e/h=0.27, being the other cases substantially similar to this one. Also in this case, the brick/mortar interface is allowed to open but not to slide. The macroscopic response of the model is similar to that represented in Fig. 10, with a long linear response up to 95% of the limit load and a sudden collapse at a total load of 82.4 kN, very close to the experimental value of 78.8 kN. The major difference arises in the structural response: the real specimen showed a clear non linear response from the early stages of the loading history, Fig. 4, while the FEM model remains linear elastic up to the limit load. This is due to the FEM code damage model, which assumes a sudden drop in the stress transfer, whilst in reality this drop is gradual. Also in the numerical model the mortar joint remained undamaged till the limit point, as experimentally detected.

Fig. 13 plots the vertical and maximum tensile stresses just before the opening of the first cracks rising two observations: 1) the lines with equal vertical stress, Fig. 13 a, are not straight with irregularity close to the free side, indicating that the neutral axis, straight on the average, suffers from local stress concentrations close to the edges; 2) close to the free side of

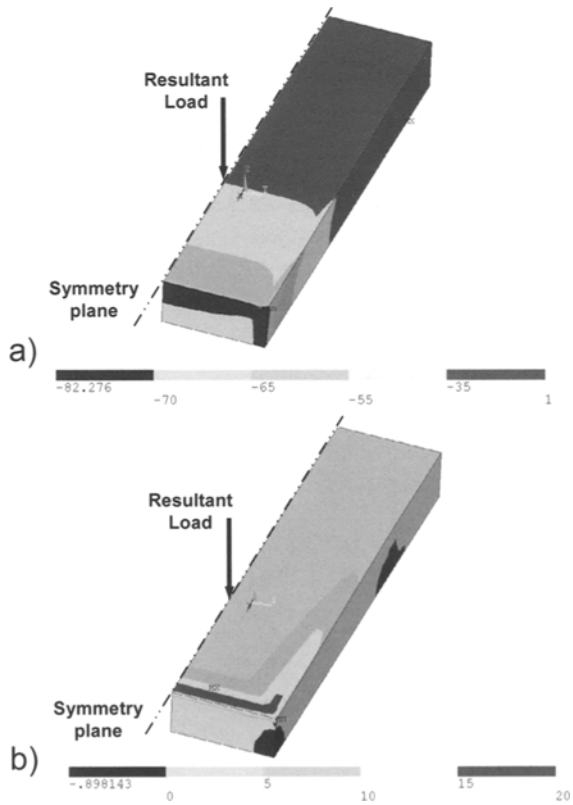

Fig. 13 - a) Vertical and b) maximum tensile stress distribution at 95% of the collapse load [N/mm^2 *10]. Upper part of the brick.

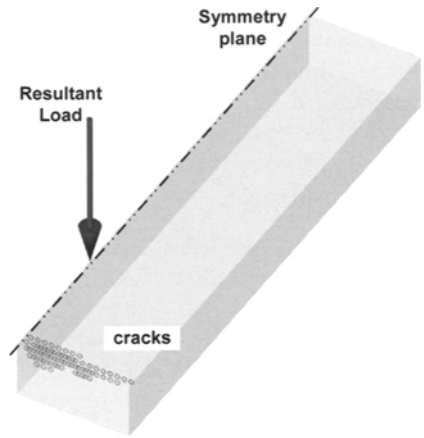

Fig. 14 - Crack distribution at 98% of the limit load. Upper part of the brick.

the compressed part of the section high tensile stresses are developed. The first cracks are developed exactly in that part starting from the symmetry axis and on the most compressed side, Fig. 14.

On the brick/mortar interface the shear stresses that are developed are quite low, never more than 0.4 N/mm^2, with an average compressive stress of 6 N/mm^2; whatever the friction coefficient at the interface, such low values of the tangential stresses justify the experimental evidence that no sliding occurs between the brick and the mortar joint.

5. COMPARISONS AND CONCLUSIONS

The experimental response of the specimen under uniform compression has been rather linear up to some 90% of the limit load. Non-uniform compressive stresses with opening of the interface, instead, exhibit clear non linear response starting from the very beginning of the loading process.

FEM models give a deeper insight in the cracking phenomenon. Cracks seem to originate at the brick/mortar interface as a consequence of the elastic mismatch between the two materials, starting on the brick side of the interface and propagating towards its centre. This evolution of the crack pattern is in agreement with some authors [26] who conjectured that the collapse mechanism is activated by some local edge effect rather than a global failure condition in the brick core. Besides, the crack pattern, position and the corresponding load level reproduced by the FEM model seem to be in reasonable agreement with experimental evidence, at least referring to the beginning of the non linear response. If the mechanical properties of the materials are evaluated by means of standard testing procedures the limit load foreseen by the FEM model is reasonably good.

The stress distribution, specifically the presence of some areas where stress concentration is found, rises some objection to the classical limit-analysis theory [18-22]. The brick tensile strength seems to be attained close to the free edges of the brick while the internal core experiences still low tensile stresses. This fact has been found on thin specimen, so that this conclusion cannot be extended to very thick eccentrically loaded masonry.

All tests with concentric loading showed that limited, but non vanishing, inelastic strains are found after the linear part of the load vs. displacement diagram. Defining the *ultimate ductility* as the ratio between the strain at collapse ε_{ul} and at the end of the elastic response ε_{el}, $\delta_{ul}=\varepsilon_{ul}/\varepsilon_{el}$, solid clay brickwork is found to have an ultimate ductility somewhere in-between 1.2-1.5. The limit domains of Fig. 15, formulated in terms of normalised eccentricity and normalised maximum axial load, show that also small values of the ultimate ductility may increase the admissible domain for internal forces (axial thrust and bending moment) so rising the load carrying capacity of an arch-type structure.

The test for concentric loading allows the actual compressive strength of the brickwork and the ultimate strain to be deduced, Fig. 4. Three different models may be formulated: a) a pure No-Tensile-Resistant (NTR) model in which a limit is set to the compressive stresses – dashed bold line in Fig. 15 b) an elastic-perfectly plastic model (see, for example, [33]) with limited ductility (δ_{ul}=1.20 and 1.42), *i.e.* in which failure is reached when the maximum compressive strain attains the ultimate value deduced in a concentric loading test – thin line in Fig. 15 c) an elastic-perfectly plastic model with unlimited ductility – solid bold line. The experimental data [10, 11], except those for solid concrete brickwork, lie somewhere in-between the NTR and Elasto-Plastic limit curves. This confirms that the effective response of masonry is something more than No-Tensile-Resistant.

An open issue is that of scale effects, which is of great importance for the extension of these results to massive masonry structures. Since the results, Fig. 15, are normalized by the concentric compressive strength, we could say that the size effect is somehow reduced in the present experimental results.

Even though the limited number of specimen does not allow a general conclusion, the experimental results showed that the assessment of an arch-type structure relying on a purely NTR model might be conservative.

Many failure theories were used to foresee the compressive

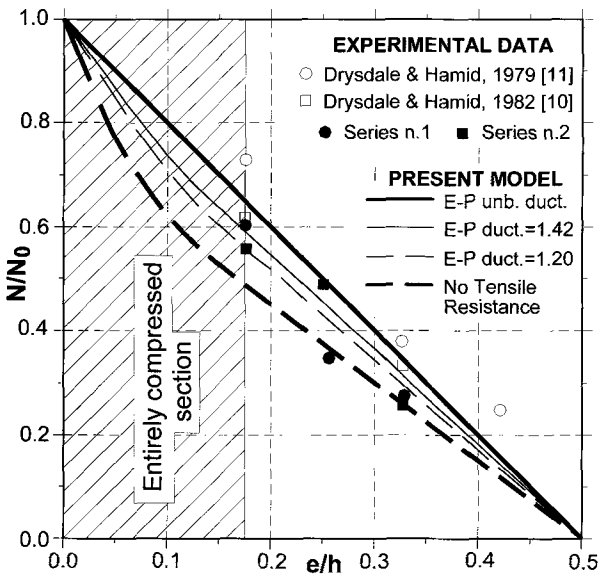

Fig. 15 - Normalized axial strength for varying eccentricity. Experimental and theoretical results.

strength of masonry. Table 5 summarizes the estimates of the compressive strength according to some of these theories and to some codes, assuming the mechanical parameters of Table 3. It has to be said that codes give characteristic values of the strength, while the comparison should be carried out relying on the average values, which are usually 20-30% higher. If the code values are multi-plied by a factor 1.2-1.3, the resulting average value is rather close to the experimental one.

Table 5 - Estimated concentric compressive strength of masonry

Reference		Notes	Compressive strength [MPa]	
Analytical	Francis [18]	elastic theory	15.0	
	Hilsdorf [19]	limit analysis	13.7	
	Khoo & Hendry [22]	limit analysis + experimental	17.8	
Design codes			**Characteristic value**	**Average value**
	Euro Code 6 [35]	-	7.4	9.6
	Fiche-UIC [36]	-	7.8	10.1
	Italian Code [37]	for M2 mortar	7.4	9.6
	Italian Code [37]	for M3 mortar	6.8	8.8
	Present work	experimental	9.9	

The results of Table 5 show that while modern codes, probably relying on a large base of experimental data, give empirical formulas which may fit well the experimental data, the limit-analysis approach somehow overestimates the actual compressive strength of masonry. Nevertheless, the estimation of the compressive strength of eccentrically loaded masonry from the geometry of the brickwork and from the mechanical properties of the components is still an open issue. For this reason, more research still needs to be carried out to widen the experimental data and to get deeper insight in the mechanisms that activate after the peak load is reached, leading to the softening phase of the non uniformly compressed specimen.

ACKNOWLEDGEMENTS

The authors acknowledge the contribution by Dott. Giovanni Mantegazza (chair of the Research Dept. - RUREDIL) and Giancarlo Sighieri (Materials Lab. - DISEG) to the experimental work, and the partial financial support of RUREDIL s.p.a., S. Donato Milanese, Italy. This research was carried out also with the partial financial support of the (MURST) Department for University and Scientific and Technological Research in the frame of the PRIN 2002/ 2003 Project "*Safety and Control of Masonry Bridges*".

REFERENCES

[1] Castigliano, C.A.P., 'Théorie de l'équilibre des systèmes élastiques et ses applications', (A.F. Negro, Torino 1879).
[2] Pippard, A.J.S. and Baker, J., 'The Voussoir Arch', in 'The Analysis of Engineering Structures', chapter 16, Pippard and Baker eds. (Edward Arnold, London, 1962) 385-403.
[3] Heyman, J., 'The masonry arch' (Ellis Horwood, Chichester, 1982).
[4] Gilbert, M., 'Ring: a 2D rigid-block analysis program for masonry arch bridges', in 'Arch'01', Proceedings of the 3rd International Arch Bridge Conference, Abdunur ed., (Presses de l'École Nationale des Ponts et Chaussées, Paris, 2001), 459-464.
[5] Hughes, T.G., 'Analysis and assessment of twin-span masonry arch bridges', *Proc. Instn. Civ. Engrs.* **110** (1995) 373-382.
[6] Crisfield, M.A., 'Finite element and mechanism methods for the analysis of masonry and brickwork arches', Transport and Road Research Laboratory, Dept. of Transport, Research Report 19 (TRL, Crowthorne, 1985).
[7] Crisfield, M.A. and Packham, A.J., 'A mechanism program for computing the strength of masonry arch bridges', Transport and Road Research Laboratory, Dept. of Transport, Research Report 124 (TRL, Crowthorne, 1988).
[8] Brencich, A. and De Francesco, U., 'Assessment of multi-span masonry arch bridges. Part I: A simplified approach. Part II: Examples and Applications', Accepted for publication in the *J. of Bridge Eng.ng, ASCE* (2003).
[9] Drysdale, R.G. and Hamid, A.A., 'Capacity of concrete block masonry prisms under eccentric compressive loading', *ACI J.nl* **80** (June 1979) 707-721.
[10] Drysdale, R.G. and Hamid, A.A., 'Effect of eccentricity on the compressive strength of brickwork', *J.nl Brit. Cer. Soc.* **30** (1982) 102-108.
[11] Drysdale, R.G., Hamid, A.A. and Baker, L.R., 'Masonry Structures, Behaviour and Design' (Prentice Hall, Englewood Cliffs, 1993).
[12] Biolzi, L., 'Evaluation of Compressive Strength of Masonry Walls by Limit Analysis', *J. Str. Eng.ng ASCE* **114** (1988), 2179-2189.
[13] Pietrusczac, S. and Niu, X., 'A mathematical description of macroscopic behavior of brick masonry', *Int. J. Sol. and Str.* **29** (1992) 531-546.
[14] Sacco E. and Marfia, S., 'Modeling of reinforced masonry elements', *Int. J.nl Sol. Str.* **38** (2001) 4177-4198.
[15] Gambarotta L. and Lagomarsino S., 'Damage models for the seismic response of brick masonry shear walls. Part I: The mortar joint model and its applications. Part II: The continuum model and its applications', *Eart. Eng. Str. Dyn.* **26** (1997) 424-462.
[16] Sacco E. and Luciano, R., 'Damage of masonry panels reinforced by FRP sheets', *Int. J.nl Sol. Str.* **35** (1998) 1723-1741.
[17] Hendry, A.W., 'Structural Brickwork' (John Wiley, New York, 1981).
[18] Francis, A.J., Horman, C.B., Jerrems, L.E., 'The effect of joint thickness and other factors on the compressive strength of brickwork', Proceedings of the 2nd International Brick Masonry Conference, Stoke on Kent (1971), 31-37.
[19] Hilsdorf, H.K., 'Investigation into the failure mechanism of brick masonry under axial compression', in *Designing, Eng.ng & Construction with Masonry Products*, F.B. Johnson ed. (Gulf Publishing, Houston, Texas, 1969), 34-41.
[20] Atkinson, R.H., Noland, J.L., 'A proposed failure theory for brick masonry in compression', Proceedings of the 3rd Canadian Masonry Symposium, Edmonton, (1983), 5/1-5/17.
[21] Shrive, N.G., 'A fundamental approach to the fracture of masonry', Proceedings of the 3rd Canadian Masonry Symposium, Edmonton, (1983), 4/1-4/16.
[22] Khoo, C.L., Hendry, A.W., 'A failure criteria for brickwork in axial compression', Proceedings of the 3rd International Brick Masonry Conference, Essen, (1973), 141-145.
[23] Page, A., Brooks, D., 'Load bearing masonry – A review', Proceedings of the 7th International Brick Masonry Conference, Melbourne (1985) 81-100.

[24] Maurenbrecher, A.H.P., 'Compressive strength of eccentrically loaded masonry prisms', Proceedings of the 3rd Canadian Masonry Symposium, Edmonton, (1983), 10/1-10/13.
[25] Taylor, N. and Mallinder, P., 'The brittle hinge in masonry arch mechanism', *The Str. Eng.* **71** (1993), 359-366.
[26] Rots, J.G., 'Numerical simulation of cracking in structural masonry, *Heron* **36** (1991) 49-63.
[27] Brencich, A. and Gambarotta, L., 'Isotropic damage model with different tensile-compressive response for brittle materials', *Int. J.nl Sol. Str.* **38** (2001) 5865-5892.
[28] Binda, L., Mirabella Roberti, G., Tiraboschi, C. and Abbaneo, S., 'Measuring masonry material properties', Proceedings of the U.S.-Italy Workshop on Guidelines for Seismic Evaluation and Rehabilitation of Unreinforced Masonry Buildings, section VI (1994), 6/3-6/24.
[29] Atkinson, R.H., Noland, J.L. and Abrams, D.P., 'A deformation failure theory for stack bond prisms in compression', Proceedings of the 7th International Brick Masonry Conference, Melbourne (1985) 577-592.
[30] van Mier, J.G.M., 'Fracture Processes of Concrete: Assessment of Material Parameters for Fracture Models' (CRC Press, Boca Raton, 1996).
[31] Rabaioli, R., 'Control methods for masonry arch bridges: an example', *Ing. Ferr.* (August 1993) 531-537 [only available in Italian].
[32] Willam, K. and Warne, E.D., Constitutive model for the triaxial behaviour of concrete, Proc. IABSE, Vol. 19, ISMES, Bergamo (1975) 19/1-19/30.
[33] Lourenço, P.B. and Rots, J.G., 'An anisotropic failure criterion for masonry suitable for numerical implementation', *Mas. Soc. J.* **18** (2000) 11-18.
[34] Brencich, A., De Francesco, U. and Gambarotta, L., 'Elastic no tensile resistant – plastic analysis of masonry arch bridges as an extension of Castigliano's method', Proceedings 9th Canadian Masonry Symposium, Fredericton (2001).
[35] ENV 1996-1-1 March 1998 – 'EURO CODE 6, Design of masonry structures, Part 1-1: General rules for buildings – Rules for reinforced and un-reinforced masonry' (1998).
[36] FICHE-UIC 778-3E, 'Recommandations pour l'évaluation de la capacité portante des ponts-voûtes existants en maçonnerie et béton' (1994).
[37] Department of Public Works, 'Technical code for design, building and assessment of masonry buildings and their strengthening' (1987) [only available in Italian].